NANO LETTERS

pubs.acs.org/NanoLett Letter

Ferroelectric Modulation of Surface Electronic States in $BaTiO_3$ for Enhanced Hydrogen Evolution Activity

Pedram Abbasi, Matthew R. Barone, Ma. de la Paz Cruz-Jáuregui, Duilio Valdespino-Padilla, Hanjong Paik, Taewoo Kim, Lior Kornblum, Darrell G. Schlom, Tod A. Pascal,* and David P. Fenning*

Cite This: https://doi.org/10.1021/acs.nanolett.2c00047 Read Online

ACCESS | Metrics & More | Article Recommendations | Supporting Information

ABSTRACT: Ferroelectric nanomaterials offer the promise of switchable electronic properties at the surface, with implications for photo- and electrocatalysis. Studies to date on the effect of ferroelectric surfaces in electrocatalysis have been primarily limited to nanoparticle systems where complex interfaces arise. Here, we use MBE-grown epitaxial $BaTiO_3$ thin films with atomically sharp interfaces as model surfaces to demonstrate the effect of ferroelectric polarization on the electronic structure, intermediate binding energy, and electrochemical activity toward the hydrogen evolution reaction (HER). Surface spectroscopy and *ab initio* DFT +U calculations of the well-defined (001) surfaces indicate that an upward polarized surface reduces the work function relative to downward polarization and leads to a smaller HER barrier, in agreement with the higher activity observed experimentally. Employing ferroelectric polarization to create multiple adsorbate interactions over a single electrocatalytic surface, as demonstrated in this work, may offer new opportunities for nanoscale catalysis design beyond traditional descriptors.

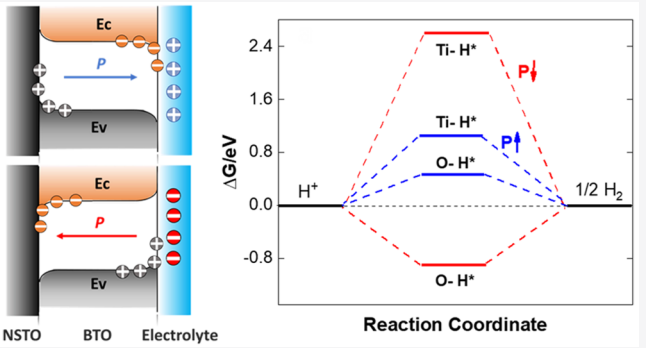

KEYWORDS: *Ferroelectrics, Electrocatalysis, Spectroscopy, Density functional theory*

INTRODUCTION

Catalyst design for chemical and energy conversion processes relies on the Sabatier principle, which states that an ideal catalyst possesses a binding strength with reaction intermediates that should be strong enough to enable reactivity, but not so strong that it poisons the active site.[1,2] While this principal descriptor has proven powerful in the design of improved catalysts and electrocatalysts, it is predicated on a particular catalyst having a singular binding interaction with key reaction intermediates that dominates its activity. One possible route to break the single-surface design constraint is the application of nanoferroelectrics, which present two distinct chemical surfaces, depending on the polarization direction.[3−5] This unique property makes ferroelectrics a particularly interesting case for catalysis, where the combination of an internal electric field and a switchable surface chemistry could potentially broaden catalyst design beyond a simple Sabatier framework.[3,4,6,7]

To date, there have been various attempts using ferroelectrics for heterogeneous catalysis, including catalysis on bare ferroelectric surfaces as well as catalysts on ferroelectric supports.[8−15] Early experiments demonstrated a dependence on the direction of ferroelectric polarization in the adsorption of small molecules on some niobate (e.g., $LiNbO_3$, $KNbO_3$)[13,16−18] and titanate (e.g., $Pb(Zr,Ti)O_3$)[3,12] surfaces. These works sparked further investigations on the role of ferroelectricity on the surface charge density,[19−21] surface reconstruction,[22−25] and chemical stability[26,27] of ABO_3 ferroelectric perovskites using spectroscopic and computational methods. In addition to bare ferroelectric surfaces, more recent studies have considered heterostructures, where ferroelectric materials are used as a catalyst support for adsorption/desorption reactions: for example, Pt and Pd thin films atop ferroelectrics ($LiNbO_3$[16,28] and $PbTiO_3$[12]) or transition-metal oxides (TiO_2[29], RuO_2,[3] or CrO_2[4]) introduced atop ferroelectric substrates. Most of these studies have been limited to computational efforts, however, mainly due to the challenges in discerning the direct effect of the ferroelectric polarization when catalyst overlayers are used. This, in turn, is due to the tendency of metal skin layers to agglomerate,[14,17] as well as the possibility of screening the effect of a ferroelectric support by high-dielectric catalysts.[20,30]

Received: January 5, 2022
Revised: April 22, 2022

https://doi.org/10.1021/acs.nanolett.2c00047
Nano Lett. XXXX, XXX, XXX−XXX

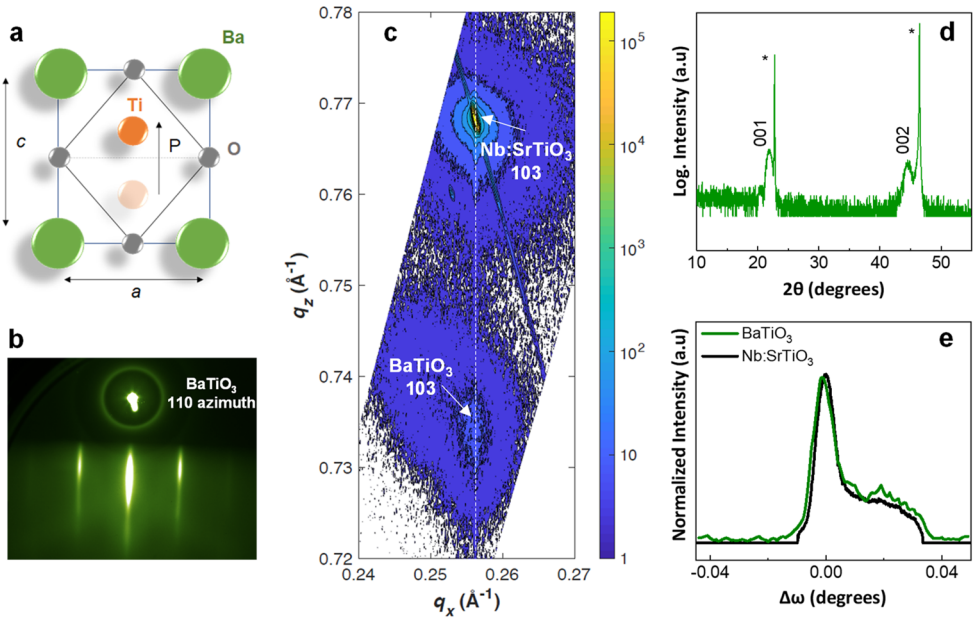

Figure 1. Structural characteristics of the (001)-oriented $BaTiO_3$ films on Nb:$SrTiO_3$: (a) schematic of a tetragonal $BaTiO_3$ unit cell with the Ti atom moving from a downward-poled to an upward-poled position in the oxygen coordination octahedron; (b) RHEED pattern of $BaTiO_3$ films viewed along the [110] azimuth; (c) RSM map of an epitaxial $BaTiO_3$/Nb:$SrTiO_3$ film showing the 103 reflections of both the film and substrate; (d) XRD θ–2θ scans of $BaTiO_3$ films (substrate peaks are denoted by *); (e) rocking curve of the film and substrate (002) peak.

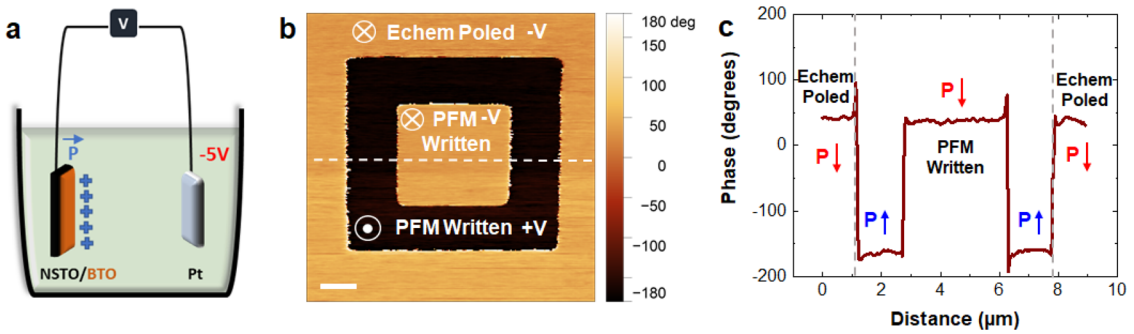

Figure 2. Electrochemical switching of ferroelectric polarization in $BaTiO_3$ (BTO) thin films: (a) schematic of the electrochemical poling method; (b) PFM phase image and (c) corresponding phase line profile of the film first poled downward over the full area by the electrochemical (Echem) method and then repoled upward and downward using the grounded PFM tip over decreasingly small square areas centered in the image. The scale bar is 1 μm.

Ferroelectric perovskites have also been an interesting class of nanomaterials for photocatalysis, since their internal electric field can be used to enhance electron–hole separation.[29,31−36] As a recent example, improved photocatalytic oxygen evolution activity has been reported using both bare ferroelectric (e.g., $BaTiO_3$,[31] $BiFeO_3$[32,37]) films and ferroelectric-supported catalysts, such as RuO_2/$BiFeO_3$.[30] In these studies the heterostructure was used as a photoanode, where ferroelectric polarization enhanced the accumulation of photogenerated holes near the surface to facilitate water oxidation.

In electrocatalysis, the implementation of ferroelectrics have been mainly limited to nanoparticles (e.g., $Bi_{0.5}Na_{0.5}TiO_3$[38] and $Bi_4Ti_3O_{12}$–$BiCoO_3$ mixtures[35]) for water splitting and the oxygen evolution reaction (OER).[39] We note that the major challenge for using nanoparticle ferroelectrics for electrocatalysis is the inherent challenge in switching the polarization, due to the need for large coercive fields and also to the less well-defined catalytic interface. Thus, despite the promise of these previous works, there remains a lack of clarity regarding the direct effect of ferroelectric switching on catalysis at the nanoscale, in part because of the complexities in establishing the polarization state on a well-defined catalytic surface that can be reasonably compared with computational models.[40]

In this work, we overcome many of these challenges by fabricating epitaxial single crystalline (001) $BaTiO_3$ ferroelectric thin films (15 nm thick) to investigate the effect of polarization switching on electrochemical hydrogen evolution as a model reaction.[41] We use an electrochemical poling technique to establish a well-defined polarization state in the thin film, without the need for a metallic overlayer. Critically, the smooth surface of nanostructured thin films grown by molecular-beam epitaxy (MBE) along with a controlled chemistry, orientation, and polarization allow us to thoroughly investigate the effect of ferroelectric switching on the reaction mechanism and surface characteristics at the nanoscale. Integrating electrochemical experiments, surface spectroscopy, and theory, we show controlled modulation of the intermediate binding energy and the electrochemical activity on the (001) $BaTiO_3$ catalyst by switching the direction of the ferroelectric polarization. The demonstrated ability to

https://doi.org/10.1021/acs.nanolett.2c00047
Nano Lett. XXXX, XXX, XXX−XXX

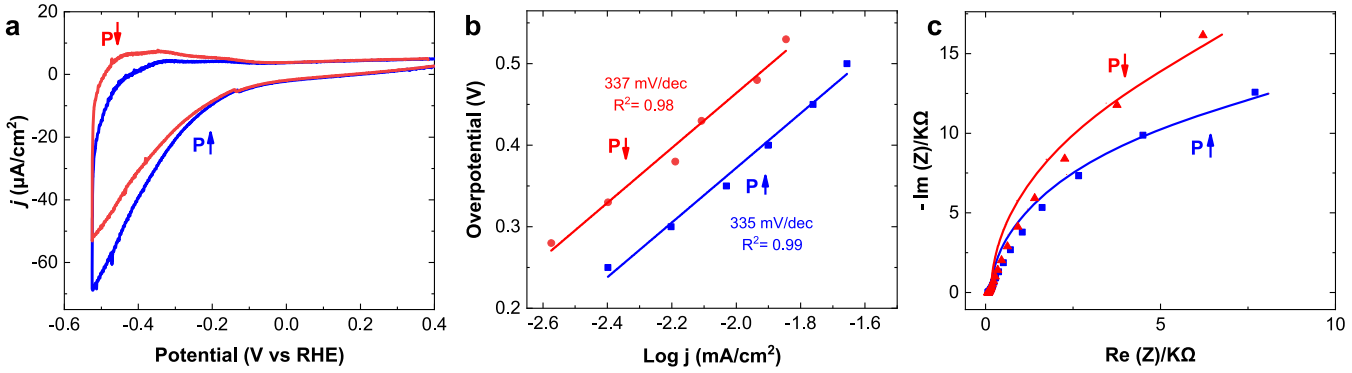

Figure 3. Electrochemical hydrogen evolution as a function of ferroelectric polarization, where data from a catalyst surface with upward polarization is shown in blue and downward polarization in red: (a) cyclic voltammetry and (b) potentiostatic Tafel analysis for upward- and downward-poled films. (c) electrochemical impedance spectra in the Faradaic region (−0.48 V vs RHE) indicating charge-transfer resistance. All data were collected in 0.1 M phosphate buffer.

modulate adsorbate binding energies on a single catalyst by ferroelectric switching opens a new dimension for catalyst electronic structure design.

RESULTS AND DISCUSSION

Epitaxial single-crystal $BaTiO_3$ thin films were grown on 0.5 wt % Nb-doped (001)-oriented $SrTiO_3$ substrates by reactive MBE at 850 °C. Surface and bulk structural characterization of the synthesized films is shown in Figure 1. A reflection high-energy electron diffraction (RHEED) image taken along the $BaTiO_3$ [110] azimuth during the growth of the film shows high contrast, well-defined 110 diffraction streaks indicating the synthesis of a smooth and epitaxial $BaTiO_3$ film (Figure 1b). Reciprocal space mapping (RSM) of the 103 reflections of both the film and substrate shows that the $BaTiO_3$ film is commensurately strained, maintaining the same in-plane lattice parameter as the substrate (Figure 1c). The specular $\theta-2\theta$ X-ray diffraction (XRD) pattern further confirms that the films are epitaxial, single-phase, and (001)-oriented (Figure 1d). The positions of $BaTiO_3$ (001) and (002) peaks are in agreement with previous reports on epitaxial $BaTiO_3$.[42] Rocking curves of the (002) peaks measured for both the $BaTiO_3$ film and the Nb:$SrTiO_3$ substrate match closely, indicating the low mosaicity of the film, as anticipated for a commensurate thin film with a low dislocation density.

To investigate the effect of polarization switching on the electrochemical performance of $BaTiO_3$ films, we used steady-state biasing at ±5 V in a nonaqueous electrolyte to switch the ferroelectric polarization in the $BaTiO_3$ films (Figure 2a). Critically, this polarization is accomplished without the application of metallic contacts atop the catalyst surface. The high electron density at the metal surface would screen any effect of the ferroelectric polarization on surface chemistry.[43] By exceeding the coercive field across the catalyst, we expected to achieve a polarization reversal across the whole surface, readying the polarized surface for an evaluation of its catalytic properties. We intentionally chose a bias slightly larger than the established coercive field for similar thin films[44] to compensate for Ohmic drops inside the electrolyte and to ensure we can reach saturation in polarization. Moreover, polarization in a nonaqueous electrolyte avoids surface reactions at such high voltages.

Piezoresponse force microscopy (PFM) reveals that this electrochemical poling produces a homogeneously polarized sample surface (Figure 2b, outer regions). In contrast, PFM phase and amplitude images of as-grown films reveal a random orientation of ferroelectric domains after synthesis, as expected (Figure S1). For the electrochemically poled sample, using the PFM tip to directly bias the sample surface locally, we repoled a smaller, selected area in the out-of-plane direction (Figure 2b, square contained by the perimeter of the dark region). Repoling an even smaller area inside the first PFM-written square with negative bias (−8 V) yielded a phase similar to that of the starting condition, confirming that the electrochemical poling had successfully saturated the polarization. The observed phase images, as well as horizontal line profiles across these areas (Figure 2c), show a phase contrast of ∼180°, confirming the successful writing of domains with an opposite out-of-plane orientation on $BaTiO_3$ films. More details on PFM experiments are presented in Figures S1 and S2 in the Supporting Information. These measurements confirmed that the electrochemical biasing poled the films homogeneously, a requirement to isolate the effect of polarization switching on electrocatalysis and surface chemistry.

The direction of the ferroelectric polarization has a distinct effect on the electrochemical characteristics of $BaTiO_3$, altering the onset potential, exchange current density, and charge transfer resistance for the hydrogen evolution reaction (HER). Electrochemical measurements were conducted in a three-electrode cell using an Ag/AgCl reference electrode, a graphite rod counter electrod,e and a near-neutral-pH electrolyte. As shown in Figure 3a, the poled-up surface shows both an earlier onset and a higher cathodic current under HER conditions, in comparison to the downward-poled sample. The Tafel analysis in Figure 3b of potentiostatic chronoamperometry reveals a distinct increase in the exchange current density on the poled-up film and a statistically insignificant change in slope. Complete chronoamperometry data are given in Figure S3. Our results show a Tafel slope of ∼335 mV/dec for both polarization states. This suggests slower HER kinetics on the $BaTiO_3$ surface in comparison with traditional HER electrocatalysts: e.g., metal oxides or noble metals with Tafel slope values of 40−120 mV/dec depending on the governing mechanism. The slow kinetics of the HER and high Tafel slopes for our catalysts may be due to the intrinsic catalytic properties of $BaTiO_3$ and also the implementation of a near-neutral buffer electrolyte[45,46] and are in agreement with limited HER activity and Tafel slopes previously reported for TiO_2-based catalysts.[47,48]

https://doi.org/10.1021/acs.nanolett.2c00047
Nano Lett. XXXX, XXX, XXX−XXX

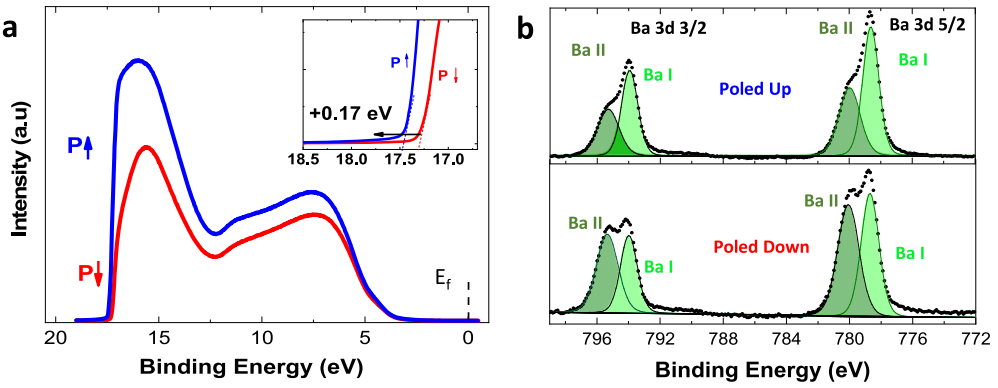

Figure 4. Angle-resolved XPS and UPS measurements: (a) valence-band UPS spectra at a 90° takeoff angle on upward and downward films showing full spectra and (inset) secondary electron cutoff; (b) X-ray photoelectron spectroscopy at a 90° takeoff angle for upward- and downward-poled films at the Ba 3d core level.

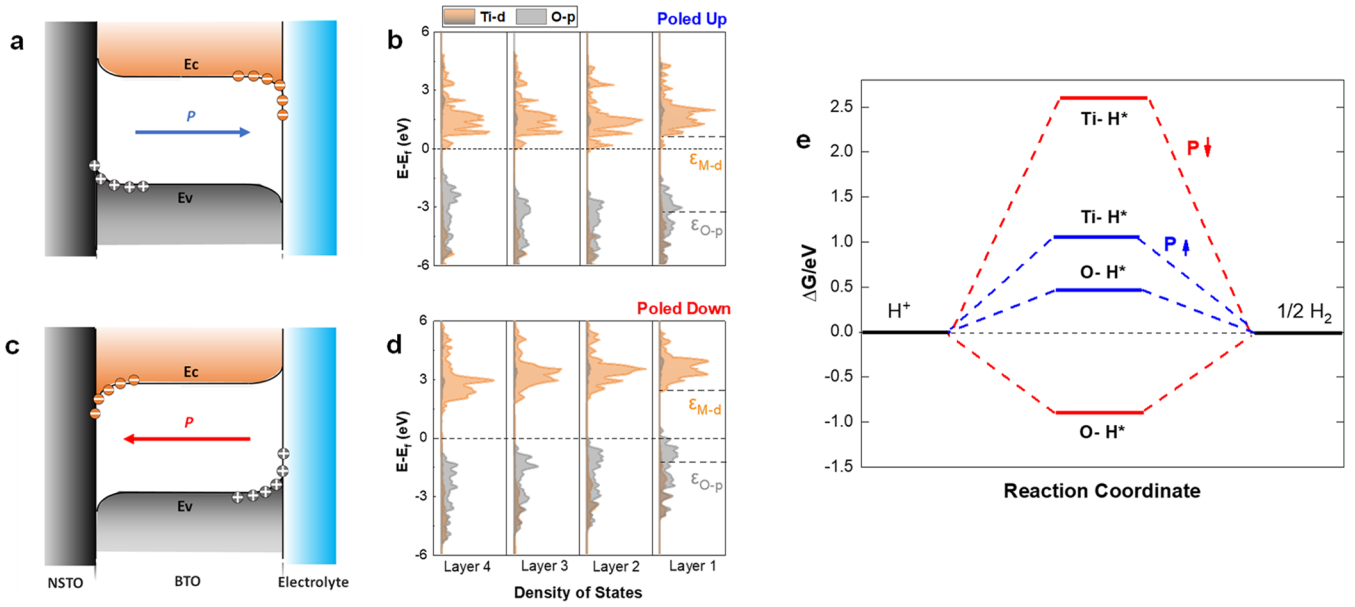

Figure 5. *Ab initio* calculations using the DFT+U approximation on polarized $BaTiO_3$ heterostructures. Band-bending schematic and layer-by-layer pDOS of Ti d and O p states from the first to the fourth atomic layers from the surface for TiO_2-terminated (001) slabs in relaxed for (a, b) upward and (c, d) downward polarization (e) Reaction free energy for H_2 formation for upward (blue- and downward-poled (red) surfaces.

Furthermore, under Faradaic reaction conditions the charge transfer resistance decreased 40% when the polarization was switched from downward to upward, as shown in Figure 3c, decreasing from 46.3 to 27.6 kΩ at −0.48 V vs RHE.

The $BaTiO_3$ catalyst was stable during the HER. H_2 was the only product detected after 60 min of a potentiostatic HER using headspace sampling and offline gas chromatography, with a Faradaic efficiency of 93.4 ± 5.2% (Table S1). Additionally, no change was observed in cyclic voltammograms obtained before and after chronoamperometry measurements (Figure S4). In short, we observed a clear modulation of the electrochemical performance of $BaTiO_3$ with a change in ferroelectric polarization, with the upward-polarized surface exhibiting a higher exchange current density and a lower charge transfer resistance.

Surface-sensitive angle-resolved X-ray photoelectron spectroscopy (AR-XPS) and ultraviolet photoelectron spectroscopy (UPS) indicate a pronounced change in the catalyst surface chemistry and electronic structure to a more reduced, electron-rich surface when the polarization is upward. UPS and valence band (VB) XPS show a distinctly larger VB density of states (DOS) at the upward-polarized surface (Figure 4a shows the UPS and Figure S5 the corresponding VB XPS). The work function is also 170 meV smaller for the upward-polarized surface in comparison to the downward-poled surface, as indicated by the secondary electron cutoff energies (Figure 4a inset).

Angle-resolved XPS indicated that the direction of ferroelectric polarization did not shift the absolute peak positions in core-level XPS spectra considerably; rather, it affected the relative peak intensities of the dominant peaks, especially in the Ba 3d spectra. This change in Ba chemical state can be seen on comparison of the spectra on upward and downward poled samples at a 90° takeoff angle (Figure 4b). The peak positions and intensities are given in Tables S2−S4, and XPS survey scans are provided in Figure S6. Previous studies on $BaTiO_3$ thin films have shown a particular sensitivity of Ba 3d core levels to the surface atomic coordination and charge density.[49−51] There are two different core level features due to Ba 3d spin−orbit coupling: a low-binding-energy feature,

https://doi.org/10.1021/acs.nanolett.2c00047
Nano Lett. XXXX, XXX, XXX−XXX

denoted Ba I, attributed to BaO in the $BaTiO_3$ lattice, and a high-binding energy-feature (Ba II), attributed to a surface peroxide chemical state (BaO_2).[52] In our experiments the intensity of the reduced Ba I peak (light green), relative to Ba II (dark green), is greater in the upward-polarized surface, in both 90 and 20° spectra (Figures S7 and S8), suggesting a higher electron density over several unit cells near the surface for the poled-up sample in comparison to the poled-down sample. This interpretation is consistent with previous studies employing X-ray reflectivity (XRR),[49] which associated the high-intensity surface peak on epitaxial $BaTiO_3$ thin films to Ba II, due to lower electron density near the surface. Additionally, high-resolution XPS measurements on the O 2p and Ti 2p core levels at 90 and 20° takeoff angles were performed and are presented in detail in Figures S7 and S8. Here, we find that the peak positions and the relative peak intensities in the Ti 2p and O 1s spectra showed only very small changes upon polarization switching in comparison with Ba 3d core levels. Previous theoretical studies have revealed a greater reduction of valence charge on Ti in comparison with Ba states in the perovskite $BaTiO_3$ structure.[53] Specifically, it has been shown that Ti cations possess a valence charge of ∼+2.5 instead of a theoretical value of +4, while the Ba states have more ionic character with an oxidation state closer to its ideal value of +2.[53,54] We believe that the greater ionicity of Ba in the perovskite structure can explain its greater sensitivity to applied electric fields and polarization switching in core-level measurements.[53,54]

Ab initio DFT calculations, using the GGA+U approximation, were performed to elucidate the atomistic mechanism behind the change in electrocatalytic activity of the ferroelectric catalyst as a function of polarization and to facilitate interpretation of the core-level XPS and valence band UPS measurements, as detailed in the Supporting Information. We find that the polarization direction has a significant effect on the position of the conduction and valence band densities of states at the surface. Figure 5 shows schematic band diagrams for upward- and downward-polarized films (Figure 5a,c) on the basis of calculations of the layer-by-layer resolved partial density of states (pDOS) for polarized (001) $BaTiO_3$ slabs (Figure 5b,d). For the upward-poled film, our calculations revealed an electron-rich surface due to the overlap of Ti d conduction band states with the Fermi level and downward band bending. Conversely, when the sample is downward-polarized, the calculations indicate a hole-doped surface as a result of an overlap between O p valence states with the Fermi level and upward band bending. Downward band bending is also evident on the basis of the positions of surface Ti d and O p band centers, where switching the polarization from downward to upward in $BaTiO_3$ shifts the Ti d band center down toward the Fermi level while it downshifts the O p band center away from the Fermi level (Table S6). The change in the position of the Fermi level at the catalytic surface upon polarization switching is in agreement with the different work functions and electron densities at the poled-up and poled-down surfaces seen spectroscopically. To further understand how the shift of the surface electronic states with polarization affects hydrogen binding, we calculated the binding energy of H* on different surface sites of the (001) $BaTiO_3$ surface (Figures S9−S12).

Our surface energy calculations (Table S5) on different surface structures of $BaTiO_3$ shows TiO_2-terminated slabs as the most stable surfaces for $BaTiO_3$. This is in agreement with earlier studies in which the dominance of TiO_2 surface planes under near-ambient conditions for (001) $BaTiO_3$ films was demonstrated.[26,55] Complementary calculations on BaO-terminated slabs shows trends similar to those for the TiO_2-terminated system, only with larger barriers. Thus, going forward we will only consider the mechanism on TiO_2-terminated slabs (Figure 5e).

As was noted earlier, on the basis of the Sabatier principle, an optimal HER catalyst should have a $|\Delta G_{H^*}|$ value close to zero. Our calculations show an uphill barrier for HER in all cases except adsorption on H* on the O site of poled-down surface. It is also evident that the poled-up surfaces show smaller reaction barriers on both the Ti and O adsorption sites, making it a more suitable surface for the HER in comparison with poled-down surfaces.[56] This result is in agreement with the downward band bending for poled-up films and higher density of electrons near the surface to facilitate a reduction reaction.

Our experimental and computational findings show that the smaller magnitude of $|\Delta G_{H^*}|$ and higher density of electrons near the surface of the poled up surface lead to a superior performance in electrochemical experiments. While a rather large modulation on binding energies is predicted by DFT calculations, it should be noted that under experimental conditions other parameters, such as the presence of an interfacial dead layer,[57] the presence of vacancies at the surface,[26] or other surface reconstructions in the aqueous electrolyte may lead to screening of the ferroelectric effect at the surface of the catalyst and reduce the ferroelectric modulation of the electrocatalytic performance. The DFT calculations provide qualitative agreement with the experimental trends seen as a result of polarization switching.

It is also evident that the inferior intrinsic properties of $BaTiO_3$ as an electrocatalyst ultimately limits its activity toward the HER. Introducing an integrated catalyst layer (e.g., transition-metal oxides such as rutiles and perovskites) on top of a ferroelectric with high remanent polarization, such as $BaTiO_3$, is thus a rational direction for future studies. Such a "catalyst-on-ferroelectric" heterostructure takes inspiration from heterostructure architectures in photocatalytic devices,[56] optoelectronics, and solid-state memory devices[58] and should offer the potential for a multidimensional catalyst design space where the polarization, chemistry, and thickness of the ferroelectric layer may be used to tune multiple binding energies on a single catalyst surface.

CONCLUSION

In this work, we demonstrate that modulating the polarization state of a ferroelectric electrocatalyst can be used to reversibly switch between two distinct electrocatalytic surfaces on a single catalyst. A polarization-dependent electrochemical activity toward the HER was demonstrated using well-defined epitaxial ferroelectric $BaTiO_3$ thin films. Upward polarization of $BaTiO_3$ leads to a higher exchange current density and a lower charge transfer resistance, arising from a lowered work function and a shift of the Ti d band center toward the Fermi level for the upward-polarized surface. DFT+U calculations indicate that switching the polarization results in a free energy barrier smaller in magnitude for the poled-up surface. The findings demonstrate that switching a ferroelectric layer can modulate the binding energy of adsorbates in electrochemical reactions, in this case for an enhanced HER. The use of ferroelectrics in catalysis to gain dynamic control of intermediate binding

https://doi.org/10.1021/acs.nanolett.2c00047
Nano Lett. XXXX, XXX, XXX−XXX

energies at the catalytic surface opens a new route for catalyst design beyond traditional limits.

METHODS

Electrochemical Measurements. The electrochemical analyses of the catalysts were executed using a potentiostat (VSP-300, biologic). The electrochemical experiments were conducted using a three-electrode setup at room temperature and ambient pressure. For electrochemical poling, a non-aqueous electrolyte (0.1 M $LiClO_4$ in polycarbonate solvent) was used and a potential of ±5 V was applied to the sample for about 10 s to switch the polarization in $BaTiO_3$ films. Cyclic voltammetry (CV) measurements were performed on prepoled samples in a 0.1 M phosphate buffer electrolyte (pH 7.2) at voltages between −0.53 and +0.4 V vs RHE in an electrochemical cell. Ag/AgCl (in 3 M potassium chloride (KCl), Pine Research) and a graphite counter electrode (Pine Research) were used as a reference electrode and counter electrode, respectively. Electrochemical impedance spectroscopy (EIS) measurements were performed at −0.48 V vs RHE between 50 mHz and 200 kHz. More details with regard to electrochemical experiments can be found in the Supporting Information.

DFT Calculations. *Ab initio* periodic DFT+U calculations were performed using the generalized gradient approximation and ultrasoft pseudopotentials (USPP) in the Quantum espresso package.[59,60] To treat the strong on-site Coulombic interaction of localized electrons, we used U = 4 eV for the Ti d states, which was previously shown to be effective in correcting artifacts arising from the conventional GGA method in electronic structure calculations.[61] A kinetic energy cutoff of 320 eV was used along with K-point grids of 4 × 4 × 1 in our periodic calculations. To model the $BaTiO_3$ thin films, we used a tetragonal ($P4mm$) unit cell with an lattice constants of a = 3.99 Å and c = 4.03 Å. Slabs were modeled on the basis of stoichiometric supercells consisting of four BaO and four TiO_2 layers on top of three layers of Pt as an electron reservoir. We performed binding free energy calculations on both TiO_2- and BaO-terminated slabs. More details regarding DFT calculations can be found in the Supporting Information.

ASSOCIATED CONTENT

Supporting Information

The Supporting Information is available free of charge at https://pubs.acs.org/doi/10.1021/acs.nanolett.2c00047.

Additional experimental details, materials, and methods, including details of computational methods and electrochemical measurements (PDF)

AUTHOR INFORMATION

Corresponding Authors

Tod A. Pascal − *Department of NanoEngineering, University of California San Diego, La Jolla, California 92093, United States;* orcid.org/0000-0003-2096-1143; Email: tpascal@ucsd.edu

David P. Fenning − *Department of NanoEngineering, University of California San Diego, La Jolla, California 92093, United States; Chemical Engineering Program, Department of Nanoengineering, University of California San Diego, La Jolla, California 92093, United States;* orcid.org/0000-0002-4609-9312; Email: dfenning@eng.ucsd.edu

Authors

Pedram Abbasi − *Department of NanoEngineering, University of California San Diego, La Jolla, California 92093, United States;* orcid.org/0000-0001-6835-3062

Matthew R. Barone − *Department of Materials Science and Engineering, Cornell University, Ithaca, New York 14853, United States;* orcid.org/0000-0003-1221-181X

Ma. de la Paz Cruz-Jáuregui − *Centro de Nanociencias y Nanotecnología (CNyN), Universidad Nacional Autónoma de México (UNAM), Carretera Tijuana-Ensenada Ensenada B.C. 22800, Mexico*

Duilio Valdespino-Padilla − *Centro de Nanociencias y Nanotecnología (CNyN), Universidad Nacional Autónoma de México (UNAM), Carretera Tijuana-Ensenada Ensenada B.C. 22800, Mexico; Universidad Autónoma de Baja California (UABC), Carretera Tijuana-Ensenada Ensenada B.C. 22800, Mexico*

Hanjong Paik − *Platform for the Accelerated Realization, Analysis & Discovery of Interface Materials (PARADIM), Cornell University, Ithaca, New York 14853, United States*

Taewoo Kim − *Chemical Engineering Program, Department of Nanoengineering, University of California San Diego, La Jolla, California 92093, United States;* orcid.org/0000-0002-6809-8222

Lior Kornblum − *Andrew & Erna Viterbi Department of Electrical & Computer Engineering, Technion—Israel Institute of Technology, Haifa 32000-03, Israel; The Nancy & Stephen Grand Technion Energy Program, Technion—Israel Institute of Technology, Haifa 32000-03, Israel;* orcid.org/0000-0001-6305-7619

Darrell G. Schlom − *Department of Materials Science and Engineering, Cornell University, Ithaca, New York 14853, United States; Kavli Institute at Cornell for Nanoscale Science, Ithaca, New York 14853, United States; Leibniz-Institut für Kristallzüchtung, 12489 Berlin, Germany;* orcid.org/0000-0003-2493-6113

Complete contact information is available at: https://pubs.acs.org/10.1021/acs.nanolett.2c00047

Author Contributions

D.P.F. and L.K. conceived the idea. P.A. performed electrochemical measurements, data processing, and first-principles DFT calculations. M.R.B. and H.P. performed sample synthesis and XRD characterization with advice from D.G.S. P.A. and T.K. prepared samples for spectroscopic measurements. M.P.C.-J. and D.V.-P. performed PFM measurements. T.A.P. and D.P.F. supervised computational and experimental efforts. All the authors contributed to the manuscript.

Notes

The authors declare no competing financial interest.

Additional data related to the thin-film growth is available at https://doi.org/10.34863/80nw-gm95.

ACKNOWLEDGMENTS

P.A. acknowledges the support from Nanoengineering department at UCSD for a graduate student fellowship. This research was partially supported by the NSF through the UC San Diego Materials Research Science and Engineering Center (UCSD MRSEC), Grant No. DMR-2011924. T.A.P. and D.P.F. acknowledge startup funding from the Jacob School of Engineering, UCSD. Materials synthesis was performed in a facility supported by the National Science Foundation

(Platform for the Accelerated Realization, Analysis, and Discovery of Interface Materials (PARADIM)) under Cooperative Agreement No. DMR-2039380. M.R.B. and D.G.S. also acknowledge support from the NSF under Cooperative Agreement No. DMR-2039380. Substrate preparation was performed in part at the Cornell NanoScale Facility, a member of the National Nanotechnology Coordinated Infrastructure (NNCI), which is supported by the NSF (Grant No. NNCI-2025233). The authors thank Dr. Ich Tran for his assistance with XPS and UPS measurements and Dr. Eduardo Murillo for the PFM image acquisition. This work used the Extreme Science and Engineering Discovery Environment (XSEDE) resources COMET at the San Diego Super Computing Center (SDSC) through allocations CSD622 and DDP381. This work was performed in part at the San Diego Nanotechnology Infrastructure (SDNI) at UC San Diego, a member of the National Nanotechnology Coordinated Infrastructure, which is supported by the National Science Foundation (Grant No. ECCS-1542148). XPS was conducted at the University of California, Irvine Materials Research Institute (IMRI), using instrumentation funded in part by the National Science Foundation Major Research Instrumentation Program under Grant No. CHE-1338173, and PFM studies were conducted under Grant No. CONACYT A1-S-14758-1542081). The authors thank Dr. Ich Tran for his assistance with XPS and UPS measurements and Dr. Eduardo Murillo for the PFM image acquisition. This work used the Extreme Science and Engineering Discovery Environment (XSEDE) resources COMET at the San Diego Super Computing Center (SDSC) through allocations CSD622 and DDP381. This work was performed in part at the San Diego Nanotechnology Infrastructure (SDNI) at UC San Diego, a member of the National Nanotechnology Coordinated Infrastructure, which is supported by the National Science Foundation (Grant No. ECCS-1542148). XPS was conducted at the University of California, Irvine Materials Research Institute (IMRI), using instrumentation funded in part by the National Science Foundation Major Research Instrumentation Program under Grant No. CHE-1338173, and PFM studies were conducted under Grant No. CONACYT A1-S-14758. The authors would like to also thank Katrina Goretskaya for her contributions to the design of the manuscript cover art.

REFERENCES

(1) Medford, A. J.; Vojvodic, A.; Hummelshøj, J. S.; Voss, J.; Abild-Pedersen, F.; Studt, F.; Bligaard, T.; Nilsson, A.; Nørskov, J. K. From the Sabatier Principle to a Predictive Theory of Transition-Metal Heterogeneous Catalysis. *J. Catal.* **2015**, *328*, 36.

(2) Koper, M. T. M.; Bouwman, E. Electrochemical Hydrogen Production: Bridging Homogeneous and Heterogeneous Catalysis. *Angew. Chemie - Int. Ed.* **2010**, *49*, 3723.

(3) Garrity, K.; Kakekhani, A.; Kolpak, A.; Ismail-Beigi, S. Ferroelectric Surface Chemistry: First-Principles Study of the PbTiO 3 Surface. *Phys. Rev. B - Condens. Matter Mater. Phys.* **2013**, *88* (4), 1−11.

(4) Kakekhani, A.; Ismail-Beigi, S. Ferroelectric-Based Catalysis: Switchable Surface Chemistry. *ACS Catal.* **2015**, *5* (8), 4537−4545.

(5) Cohen, R. E. Origin of Ferroelectricity in Perovskite Oxides. *Nature* **1992**, *358*, 136.

(6) Kakekhani, A.; Ismail-Beigi, S. Ferroelectric Oxide Surface Chemistry: Water Splitting via Pyroelectricity. *J. Mater. Chem. A* **2016**, *4* (14), 5235−5246.

(7) Kakekhani, A.; Ismail-beigi, S.; Altman, E. I. Ferroelectrics: A Pathway to Switchable Surface Chemistry and Catalysis. *Surf. Sci.* **2016**, *650*, 302−316.

(8) Li, D.; Zhao, M. H.; Garra, J.; Kolpak, A. M.; Rappe, A. M.; Bonnell, D. A.; Vohs, J. M. Direct in Situ Determination of the Polarization Dependence of Physisorption on Ferroelectric Surfaces. *Nat. Mater.* **2008**, *7*, 473.

(9) Yun, Y.; Li, M.; Liao, D.; Kampschulte, L.; Altman, E. I. Geometric and Electronic Structure of Positively and Negatively Poled LiNbO3 (0 0 0 1) Surfaces. *Surf. Sci.* **2007**, *601*, 4636.

(10) Garrity, K.; Kolpak, A. M.; Ismail-Beigi, S.; Altman, E. I. Chemistry of Ferroelectric Surfaces. *Adv. Mater.* **2010**, *22* (26−27), 2969−2973.

(11) Yun, Y.; Altman, E. I. Using Ferroelectric Poling to Change Adsorption on Oxide Surfaces. *J. Am. Chem. Soc.* **2007**, *129*, 15684.

(12) Kolpak, A. M.; Grinberg, I.; Rappe, A. M. Polarization Effects on the Surface Chemistry of PbTiO3-Supported Pt Films. *Phys. Rev. Lett.* **2007**, *98* (16), 3−6.

(13) Yun, Y.; Kampschulte, L.; Li, M.; Liao, D.; Altman, E. I. Effect of Ferroelectric Poling on the Adsorption of 2-Propanol on LiNbO3(0001). *J. Phys. Chem. C* **2007**, *111*, 13951.

(14) Kim, S.; Schoenberg, M. R.; Rappe, A. M. Polarization Dependence of Palladium Deposition on Ferroelectric Lithium Niobate (0001) Surfaces. *Phys. Rev. Lett.* **2011**, *107*, 076102.

(15) Kakekhani, A.; Ismail-Beigi, S. Polarization-Driven Catalysis: Via Ferroelectric Oxide Surfaces. *Phys. Chem. Chem. Phys.* **2016**, *18* (29), 19676−19695.

(16) Inoue, Y.; Yoshioka, I.; Sato, K. Polarization Effects upon Adsorptive and Catalytic Properties. 1. CO Oxidation over Pd Deposited on LiNbO3 Ferroelectrics. *J. Phys. Chem.* **1984**, *88*, 1148.

(17) Yun, Y.; Pilet, N.; Schwarz, U. D.; Altman, E. I. Comparison of the Interaction of Pd with Positively and Negatively Poled LiNbO3(0 0 0 1). *Surf. Sci.* **2009**, *603*, 3145.

(18) Parravano, G. Ferroelectric Transitions and Heterogenous Catalysis. *J. Chem. Phys.* **1952**, *20*, 342.

(19) Sanna, S.; Rode, S.; Hölscher, R.; Klassen, S.; Marutschke, C.; Kobayashi, K.; Yamada, H.; Schmidt, W. G.; Kühnle, A. Charge Compensation by Long-Period Reconstruction in Strongly Polar Lithium Niobate Surfaces. *Phys. Rev. B - Condens. Matter Mater. Phys.* **2013**, *88* (11), 1−5.

(20) Wang, J. L.; Vilquin, B.; Barrett, N. Screening of Ferroelectric Domains on BaTiO 3(001) Surface by Ultraviolet Photo-Induced Charge and Dissociative Water Adsorption. *Appl. Phys. Lett.* **2012**, *101* (9), 092902.

(21) Kalinin, S. V.; Bonnell, D. A. Local Potential and Polarization Screening on Ferroelectric Surfaces. *Phys. Rev. B - Condens. Matter Mater. Phys.* **2001**, *63* (12), 1−13.

(22) Garrity, K.; Kakekhani, A.; Kolpak, A.; Ismail-Beigi, S. Ferroelectric Surface Chemistry: First-Principles Study of the PbTiO 3 Surface. *Phys. Rev. B - Condens. Matter Mater. Phys.* **2013**, *88* (4), 1.

(23) Sanna, S.; Schmidt, W. G. Lithium Niobate X -Cut, y -Cut, and Z -Cut Surfaces from Ab Initio Theory. *Phys. Rev. B - Condens. Matter Mater. Phys.* **2010**, *81* (21), 214116.

(24) Fong, D. D.; Kolpak, A. M.; Eastman, J. A.; Streiffer, S. K.; Fuoss, P. H.; Stephenson, G. B.; Thompson, C.; Kim, D. M.; Choi, K. J.; Eom, C. B.; Grinberg, I.; Rappe, A. M. Stabilization of Monodomain Polarization in Ultrathin PbTiO3 Films. *Phys. Rev. Lett.* **2006**, *96* (12), 3−6.

(25) Cherifi, S.; Hertel, R.; Fusil, S.; Béa, H.; Bouzehouane, K.; Allibe, J.; Bibes, M.; Barthélémy, A. Imaging Ferroelectric Domains in Multiferroics Using a Low-Energy Electron Microscope in the Mirror Operation Mode. *Phys. Status Solidi - Rapid Res. Lett.* **2010**, *4* (1−2), 22−24.

(26) Kolpak, A. M.; Li, D.; Shao, R.; Rappe, A. M.; Bonnell, D. A. Evolution of the Structure and Thermodynamic Stability of the BaTiO3(001) Surface. *Phys. Rev. Lett.* **2008**, *101* (3), 036102.

(27) Gattinoni, C.; Strkalj, N.; Härdi, R.; Fiebig, M.; Trassin, M.; Spaldin, N. A. Interface and Surface Stabilization of the Polarization in Ferroelectric Thin Films. *Proc. Natl. Acad. Sci. U. S. A.* **2020**, *117* (46), 28589−28595.

https://doi.org/10.1021/acs.nanolett.2c00047
Nano Lett. XXXX, XXX, XXX−XXX

(28) Li, D.; Zhao, M. H.; Garra, J.; Kolpak, A. M.; Rappe, A. M.; Bonnell, D. A.; Vohs, J. M. Direct in Situ Determination of the Polarization Dependence of Physisorption on Ferroelectric Surfaces. *Nat. Mater.* **2008**, *7* (6), 473−477.
(29) Lee, J. H.; Selloni, A. TiO 2/Ferroelectric Heterostructures as Dynamic Polarization-Promoted Catalysts for Photochemical and Electrochemical Oxidation of Water. *Phys. Rev. Lett.* **2014**, *112* (19), 196102.
(30) Kalinin, S. V.; Kim, Y.; Fong, D. D.; Morozovska, A. N. Surface-Screening Mechanisms in Ferroelectric Thin Films and Their Effect on Polarization Dynamics and Domain Structures*. *Rep. Prog. Phys.* **2018**, *81* (3), 036502.
(31) Rioult, M.; Datta, S.; Stanescu, D.; Stanescu, S.; Belkhou, R.; Maccherozzi, F.; Magnan, H.; Barbier, A. Tailoring the Photocurrent in BaTiO 3 /Nb:SrTiO 3 Photoanodes by Controlled Ferroelectric Polarization. *Appl. Phys. Lett.* **2015**, *107* (10), 103901.
(32) Shah, J. H.; Huang, B.; Idris, A. M.; Liu, Y.; Malik, A. S.; Hu, W.; Zhang, Z.; Han, H.; Li, C. Regulation of Ferroelectric Polarization to Achieve Efficient Charge Separation and Transfer in Particulate RuO 2 /BiFeO 3 for High Photocatalytic Water Oxidation Activity. *Small* **2020**, *16* (44), 2003361.
(33) Li, Y.; Li, J.; Yang, W.; Wang, X. Implementation of Ferroelectric Materials in Photocatalytic and Photoelectrochemical Water Splitting. *Nanoscale Horizons* **2020**, *5* (8), 1174−1187.
(34) Yang, L.; Loh, L.; Nandakumar, D. K.; Lu, W.; Gao, M.; Wee, X. L. C.; Zeng, K.; Bosman, M.; Tan, S. C. Sustainable Fuel Production from Ambient Moisture via Ferroelectrically Driven MoS 2 Nanosheets. *Adv. Mater.* **2020**, *32* (25), 2000971.
(35) Li, X.; Liu, H.; Chen, Z.; Wu, Q.; Yu, Z.; Yang, M.; Wang, X.; Cheng, Z.; Fu, Z.; Lu, Y. Enhancing Oxygen Evolution Efficiency of Multiferroic Oxides by Spintronic and Ferroelectric Polarization Regulation. *Nat. Commun.* **2019**, *10* (1), 1409.
(36) Xu, X.; Xiao, L.; Jia, Y.; Wu, Z.; Wang, F.; Wang, Y.; Haugen, N. O.; Huang, H. Pyro-Catalytic Hydrogen Evolution by Ba0.7Sr0.3TiO3 Nanoparticles: Harvesting Cold−Hot Alternation Energy near Room-Temperature. *Energy Environ. Sci.* **2018**, *11*, 2198.
(37) Li, Z.; Zhao, Y.; Li, W. L.; Song, R.; Zhao, W.; Wang, Z.; Peng, Y.; Fei, W. D. Photovoltaic Effect Induced by Self-Polarization in BiFeO3 Films. *J. Phys. Chem. C* **2021**, *125* (17), 9411−9418.
(38) Kushwaha, H. S.; Halder, A.; Vaish, R. Ferroelectric Electrocatalysts: A New Class of Materials for Oxygen Evolution Reaction with Synergistic Effect of Ferroelectric Polarization. *J. Mater. Sci.* **2018**, *53*, 1414.
(39) Li, Y.; Li, J.; Yang, W.; Wang, X. Implementation of Ferroelectric Materials in Photocatalytic and Photoelectrochemical Water Splitting. *Nanoscale Horizons.* **2020**, *5*, 1174.
(40) Liang, Z.; Yan, C. F.; Rtimi, S.; Bandara, J. Piezoelectric Materials for Catalytic/Photocatalytic Removal of Pollutants: Recent Advances and Outlook. *Appl. Catal. B Environ.* **2019**, *241*, 256.
(41) Nørskov, J. K.; Bligaard, T.; Logadottir, A.; Kitchin, J. R.; Chen, J. G.; Pandelov, S.; Stimming, U. Trends in the Exchange Current for Hydrogen Evolution. *J. Electrochem. Soc.* **2005**, *152*, J23.
(42) Wagué, B.; Brubach, J. B.; Niu, G.; Dong, G.; Dai, L.; Roy, P.; Saint-Girons, G.; Rojo-Romeo, P.; Robach, Y.; Vilquin, B. Structural Studies of Epitaxial BaTiO3 Thin Film on Silicon. *Thin Solid Films* **2020**, *693*, 137636.
(43) Datta, S.; Rioult, M.; Stanescu, D.; Magnan, H.; Barbier, A. Manipulating the Ferroelectric Polarization State of BaTiO3 Thin Films. *Thin Solid Films* **2016**, *607*, 7.
(44) Jo, J. Y.; Kim, Y. S.; Noh, T. W.; Yoon, J.-G.; Song, T. K. Coercive Fields in Ultrathin BaTiO3 Capacitors. *Appl. Phys. Lett.* **2006**, *89* (23), 232909.
(45) Bao, F.; Kemppainen, E.; Dorbandt, I.; Bors, R.; Xi, F.; Schlatmann, R.; Krol, R.; Calnan, S. Understanding the Hydrogen Evolution Reaction Kinetics of Electrodeposited Nickel-Molybdenum in Acidic, Near- Neutral, and Alkaline Conditions. *ChemElectroChem* **2021**, 195−208.
(46) Yu, J.; Li, G.; Liu, H.; Zeng, L.; Zhao, L.; Jia, J.; Zhang, M.; Zhou, W.; Liu, H.; Hu, Y. Electrochemical Flocculation Integrated Hydrogen Evolution Reaction of Fe@N-Doped Carbon Nanotubes on Iron Foam for Ultralow Voltage Electrolysis in Neutral Media. *Adv. Sci.* **2019**, *6* (18), 1901458.
(47) Benson, E. E.; Ha, M.-A.; Gregg, B. A.; van de Lagemaat, J.; Neale, N. R.; Svedruzic, D. Dynamic Tuning of a Thin Film Electrocatalyst by Tensile Strain. *Sci. Rep.* **2019**, *9*, 1−8.
(48) Noor, S.; Sajjad, S.; Leghari, S. A. K.; Flox, C.; Kallio, T. Efficient Electrochemical Hydrogen Evolution Reaction and Solar Activity via Bi-Functional GO/Co3O4−TiO2 Nano Hybrid Structure. *Int. J. Hydrogen Energy* **2020**, *45* (35), 17410−17421.
(49) Li, X. L.; Lu, H. B.; Li, M.; Mai, Z.; Kim, H.; Jia, Q. J.; Li, X. L.; Lu, H. B.; Li, M.; Mai, Z. Characteristics of the Low Electron Density Surface Layer on Ba Ti O 3 Thin Films. *Appl. Phys. Chem.* **2014**, *92*, 012902.
(50) Li, X. L.; Chen, B.; Jing, H. Y.; Lu, H. B.; Zhao, B. R.; Mai, Z. H.; Jia, Q. J.; Li, X. L.; Chen, B.; Jing, H. Y.; Lu, H. B.; Zhao, B. R.; Mai, Z. H. Experimental Evidence of the " Dead Layer " at Pt/Ba Ti O 3 Interface. *Appl. Phys. Lett.* **2005**, *87* (2005), 222905.
(51) Craciun, V.; Singh, R. K. Characteristics of the Surface Layer of Barium Strontium Titanate Thin Films Deposited by Laser Ablation Characteristics of the Surface Layer of Barium Strontium Titanate Thin Films Deposited by Laser Ablation. *Appl. Phys. Lett.* **2000**, *76* (14), 1932.
(52) Chakrabarti, S.; Ginnaram, S.; Jana, S.; Wu, Z. Y.; Singh, K.; Roy, A.; Kumar, P.; Maikap, S.; Qiu, J. T.; Cheng, H. M.; Tsai, L. N.; Chang, Y. L.; Mahapatra, R.; Yang, J. R. Negative Voltage Modulated Multi-Level Resistive Switching by Using a Cr/BaTiO x/TiN Structure and Quantum Conductance through Evidence of H 2 O 2 Sensing Mechanism. *Sci. Rep.* **2017**, *7*, 4735 DOI: 10.1038/s41598-017-05059-9.
(53) Sousa, C.; Franccsc, I. Ionic-Covalent Transition in Titanium Oxides Carmcn. *Phys. Rev. B* **1994**, *50* (19), 13974.
(54) Bocquet, A. E.; Mizokawa, T.; Morikawa, K.; Fujimori, A.; Barman, S. R.; Maiti, K.; Sarma, D. D.; Tokura, Y.; Onoda, M. Electronic Structure of Early 3 d -Transition-Metal Oxides by Analysis of the 2 p Core-Level Photoemission Spectra. *Phys. Rev. B* **1996**, *53* (3), 1161−1170.
(55) Eglitis, R. I.; Vanderbilt, D. Ab Initio Calculations of BaTi O3 and PbTi O3 (001) and (011) Surface Structures. *Phys. Rev. B - Condens. Matter Mater. Phys.* **2007**, *76* (15), 1−9.
(56) Yuan, J.; Wang, C.; Liu, Y.; Wu, P.; Zhou, W. Tunable Photocatalytic HER Activity of Single-Layered TiO 2 Nanosheets with Transition-Metal Doping and Biaxial Strain. *J. Phys. Chem. C* **2019**, *123* (1), 526−533.
(57) Yang, Q.; Cao, J.; Zhou, Y.; Sun, L.; Lou, X. Dead Layer Effect and Its Elimination in Ferroelectric Thin Film with Oxide Electrodes. *Acta Mater.* **2016**, *112*, 216−223.
(58) Spreitzer, M.; Klement, D.; Parkelj Potočnik, T.; Trstenjak, U.; Jovanović, Z.; Nguyen, M. D.; Yuan, H.; ten Elshof, J. E.; Houwman, E.; Koster, G.; Rijnders, G.; Fompeyrine, J.; Kornblum, L.; Fenning, D. P.; Liang, Y.; Tong, W.-Y.; Ghosez, P. Epitaxial Ferroelectric Oxides on Silicon with Perspectives for Future Device Applications. *APL Mater.* **2021**, *9* (4), 040701.
(59) Giannozzi, P.; Baroni, S.; Bonini, N.; Calandra, M.; Car, R.; Cavazzoni, C.; Ceresoli, D.; Chiarotti, G. L.; Cococcioni, M.; Dabo, I.; Dal Corso, A.; De Gironcoli, S.; Fabris, S.; Fratesi, G.; Gebauer, R.; Gerstmann, U.; Gougoussis, C.; Kokalj, A.; Lazzeri, M.; Martin-Samos, L.; Marzari, N.; Mauri, F.; Mazzarello, R.; Paolini, S.; Pasquarello, A.; Paulatto, L.; Sbraccia, C.; Scandolo, S.; Sclauzero, G.; Seitsonen, A. P.; Smogunov, A.; Umari, P.; Wentzcovitch, R. M. QUANTUM ESPRESSO: A Modular and Open-Source Software Project for Quantum Simulations of Materials. *J. Phys.: Condens. Matter* **2009**, *21*, 395502.
(60) Giannozzi, P.; Andreussi, O.; Brumme, T.; Bunau, O.; Buongiorno Nardelli, M.; Calandra, M.; Car, R.; Cavazzoni, C.; Ceresoli, D.; Cococcioni, M.; Colonna, N.; Carnimeo, I.; Dal Corso, A.; De Gironcoli, S.; Delugas, P.; Distasio, R. A.; Ferretti, A.; Floris, A.; Fratesi, G.; Fugallo, G.; Gebauer, R.; Gerstmann, U.; Giustino, F.; Gorni, T.; Jia, J.; Kawamura, M.; Ko, H. Y.; Kokalj, A.; Kücükbenli, E.;

https://doi.org/10.1021/acs.nanolett.2c00047
Nano Lett. XXXX, XXX, XXX−XXX

Lazzeri, M.; Marsili, M.; Marzari, N.; Mauri, F.; Nguyen, N. L.; Nguyen, H. V.; Otero-De-La-Roza, A.; Paulatto, L.; Poncé, S.; Rocca, D.; Sabatini, R.; Santra, B.; Schlipf, M.; Seitsonen, A. P.; Smogunov, A.; Timrov, I.; Thonhauser, T.; Umari, P.; Vast, N.; Wu, X.; Baroni, S. Advanced Capabilities for Materials Modelling with Quantum ESPRESSO. *J. Phys.: Condens. Matter* **2017**, *29*, 465901.

(61) Ali, A.; Khan, I.; Ali, Z.; Khan, F.; Ahmad, I. First-Principles Study of BiFeO 3 and BaTiO 3 in Tetragonal Structure. *Int. J. Mod. Phys. B* **2019**, 33 (21), 1950231.

https://doi.org/10.1021/acs.nanolett.2c00047
Nano Lett. XXXX, XXX, XXX−XXX